Supplemental of

Sorption of VOCs by Polymer Tubing: Implications for Indoor Air and Use as a Simple Gas-Phase Volatility Separation Technique

Melissa Morris et al.

Correspondence to: Jose L. Jimenez (jose.jimenez@colorado.edu)

Table S1. Averaged breakdown of surface area according to material type, for 3 types of rooms, taken from Manuja et al. (2019).

Room Type	**Paint**	**Wood**	**Fabric / Fiber**	**Metal**	**Plastic**	**Glass**	**Other**
Bedroom (N=10)	49.4 %	18.2 %	21.7 %	1.4 %	3.1 %	1.7 %	4.5 %
Kitchen (N=9)	39.5 %	26.6 %	2.6 %	12.8 %	10.9 %	2.3 %	5.2 %
Office (N=3)	27.8 %	16.5 %	8.2 %	11.8 %	26.9 %	3.5 %	5.3 %

Table S2. Manufacturing information for chemicals and tubing materials used in this study.

Chemical	**SIMPOL.1 *C** (ug m^{-3})**	**Purity**	**Manufacturer**	**CAS**	**Lot #**
2-Butanone	1.65E9	99+%	Aldrich Chemical Co.	78-93-3	-
2-Pentanone	6.20E8	99+%	Aldrich Chemical Co.	107-87-9	HS 07040KN
2-Hexanone	2.33E8	98%	J&K	591-78-6	L970O51
2-Heptanone	8.77E7	99%	Aldrich Chemical Co.	110-43-0	14001MA
2-Octanone	3.30E7	98%	Aldrich Chemical Co.	111-13-7	065295Z
2-Nonanone	1.24E7	99+%	Aldrich Chemical Co.	821-55-6	08322AJ
2-Decanone	4.67E6	98%	Aldrich Chemical Co.	693-54-9	-
2-Undecanone	1.76E6	99%	Aldrich Chemical Co.	112-12-9	-
2-Dodecanone	6.61E5	99%	-	6175-49-1	-
2-Tridecanone	2.49E5	99%	Aldrich Chemical Co.	593-08-8	17197MJ
2-Tetradecanone	9.36E4	98%	CHEMSAMPCO	2345-27-9	8451.90-3
3-Hexadecanone	1.32E4	99%	CHEMSAMPCO	18787-64-9	3294.00-4

Tubing Material	**Inner Diameter (cm)**	**Length (cm)**	**Supplier (Part No.)**	**Price per foot**
Nylon	0.318	152	McMaster Carr (8628K48)	$0.88
Polyester	0.635	182	McMaster Carr (9245K17)	$1.83
Polypropylene	0.437	456	W. W. Grainger Inc. (4VXX2)	$0.33
Polyethylene	0.397	251	W. W. Grainger Inc. (4HM13)	$0.22
Conductive PFA (perfluoroalkoxy alkane)	0.476	149	Fluorostore (FO152O2G)	$6.39
Conductive PTFE (polytetrafluoroethylene)	0.380	99.5	Finemech Inc. (S1827-68)	$1.74
Conductive PUN (polyurethane)	0.595	224	Aerosol Magee Scientific	-
Conductive Silicone	0.483	117	TSI Inc. (3001788)	$15.00
Stainless Steel (SS)	0.395	61	SilcoTek Corp.	-
Dursan® Coated SS	0.395	61	SilcoTek Corp.	$3.87
SilcoNert® 2000 Coated SS	0.395	61	SilcoTek Corp.	$2.87
Silonite™ Coated SS	0.457	180	Entech Instruments	$11.48

Table S3. Detailed summary of fitting parameters in this work.

Tubing material	Mass absorptivity, C_W (µg m^{-3})	Log Diffusion Coefficient, D_f (cm^2 s^{-1})	Mass fraction availability parameter, γ (unitless)	Surface roughness parameter (unitless)	Approx. Partitioning Depth after 20 mins (µm)
cPFA (conductive perfluoroalkoxy alkane)	2.5 x 10^7	-	-	1	C_6: 0.055
cPTFE (conductive polytetrafluoroethylene)	9.3 x 10^7	-	-	1	C_6: 0.20
Nylon	3.5 x 10^7	-	-	1.4	C_6: 0.098
Polyester	2.4 x 10^7	-	-	1.3	C_6: 0.11
Polypropylene	SLM: 1.7 x 10^8 MLM: 3.0 x 10^{10} (avg. of C_6, C_8, C_{10}, C_{12})	C_6: -7.4	0.02	2.9	C_6: 110
		C_8: -8.2			C_8: 43
		C_{10}: -8.4			C_{10}: 34
		C_{12}: -8.4			C_{12}: 34
Polyethylene	SLM: 2.1 x 10^9 MLM: 3.0 x 10^{11} (avg. of C_6, C_8, C_{10})	C_6: -6.4	0.03	2.75	C_6: 340
		C_8: -6.8			C_8: 220
		C_{10}: -6.7			C_{10}: 240
cSI (conductive silicone)	SLM: 2.5 x 10^{11} MLM: 6.9 x 10^{13} (average of C_6, C_8)	C_6: -6.5	1	9.2	C_6: 310
		C_8: -6.6			C_8: 270

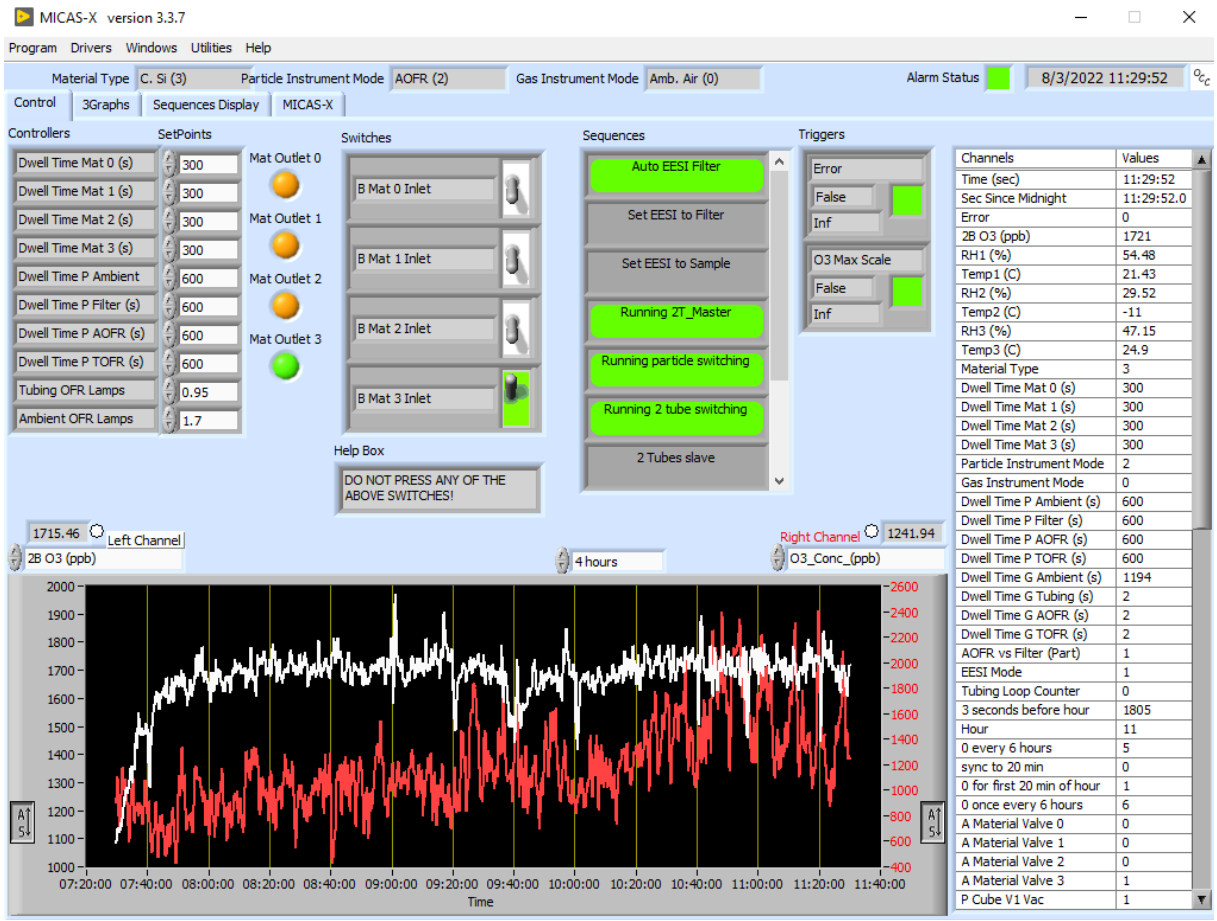

Figure S1. Screenshot of the custom user interface for the GVS acquisition software (MICAS, Original Code, Boulder, CO) within Labview. The user can control the GVS valves manually, set a dwell time for each polymer inlet, or code a more complex valve switching sequence.

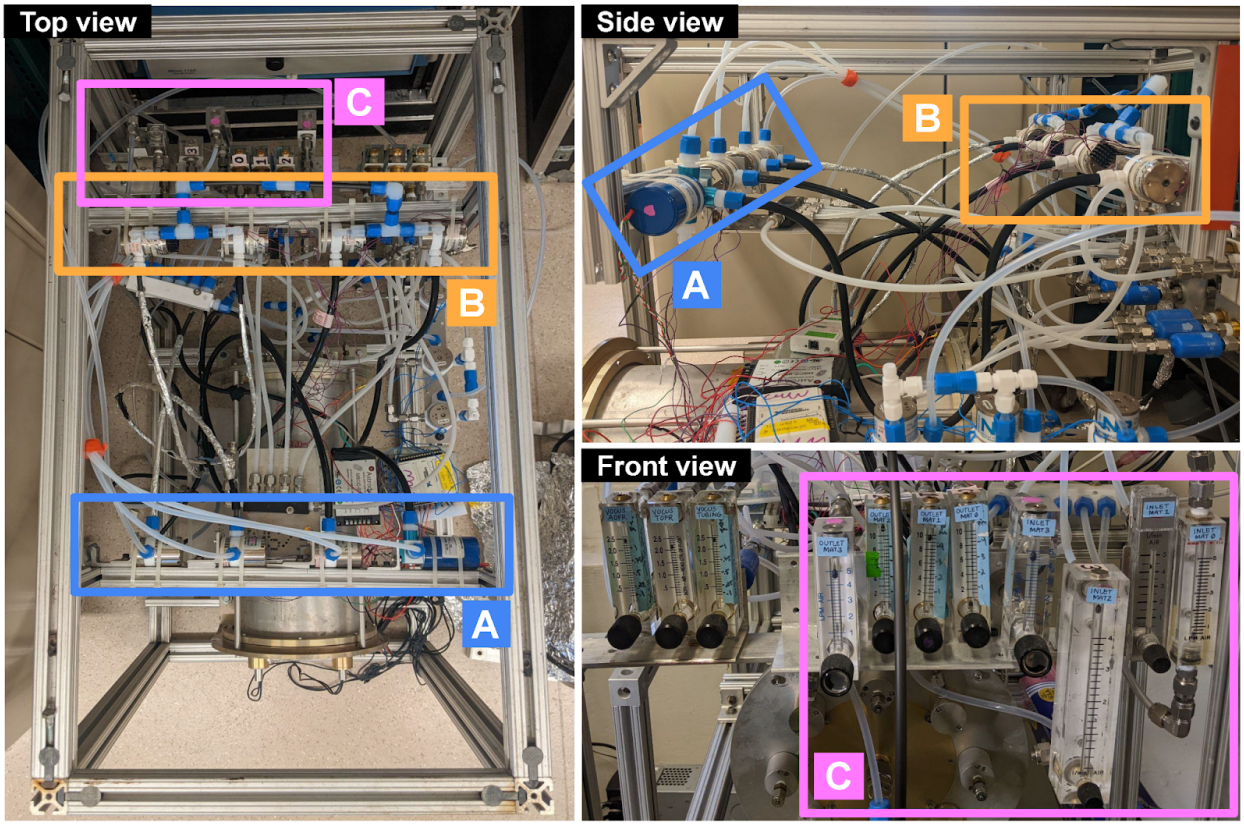

Figure S2. Top, side and front photos of the gas volatility separator (GVS), installed above an oxidation flow reactor in a rack for a field campaign. Box A contains the four 3-way inlet valves, which control whether the tubes receive ambient air or zero air. Box B contains the four 3-way outlet valves, which control whether the tubes send air to the instruments or to the exhaust. Box C contains 8 rotameters; the "inlet" rotameters show if zero air is flowing to each tube, and the "outlet" rotameters show if each tube is flowing to the exhaust. Importantly, the rotameters are not part of the main sampling pathway (when ambient air flows through the tubes to the instruments). The 3-way valves are wired to a solid state relay board, which communicates with a program written in MICAS.

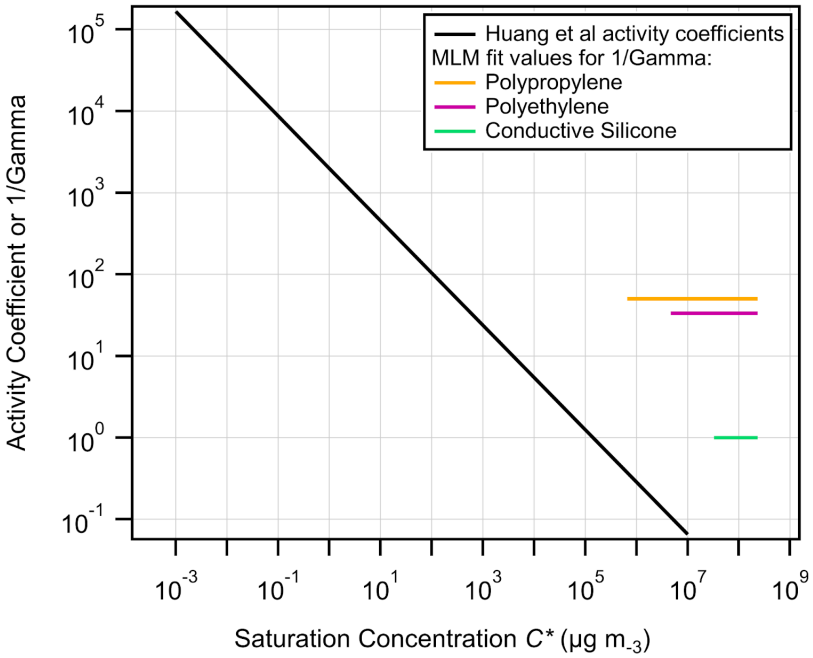

Figure S3. Activity coefficients calculated from the literature from Huan et al. (2018), plotted as a function of saturation concentration of the absorbed species, compared to the multilayer model parameter, Υ (plotted as $1/\Upsilon$). As discussed in the main text, Υ is mathematically equivalent to 1/activity coefficient.

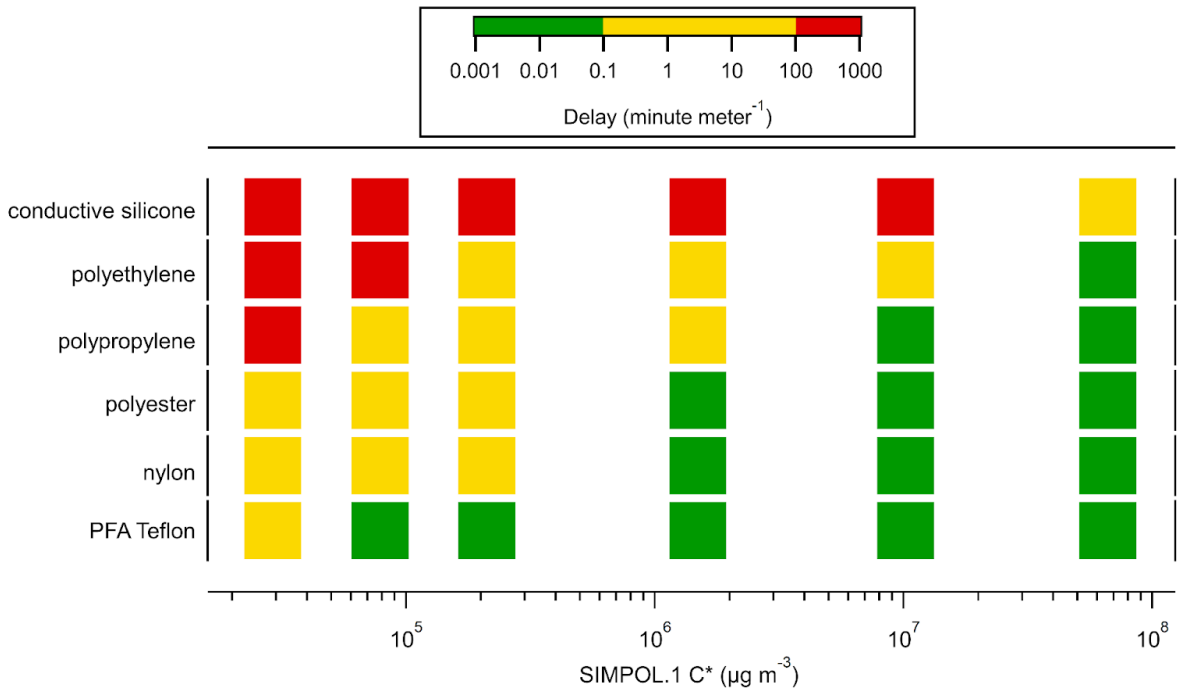

Figure S4. Experimental partitioning delay times for a series of 2-ketones through different polymer materials, simplified into a 'stop light' color scheme. Green squares indicate compounds of the plotted volatility will pass through the plotted material with minimal delays. Yellow squares indicate that significant delays will occur. Red squares indicate minimal to no transmission.

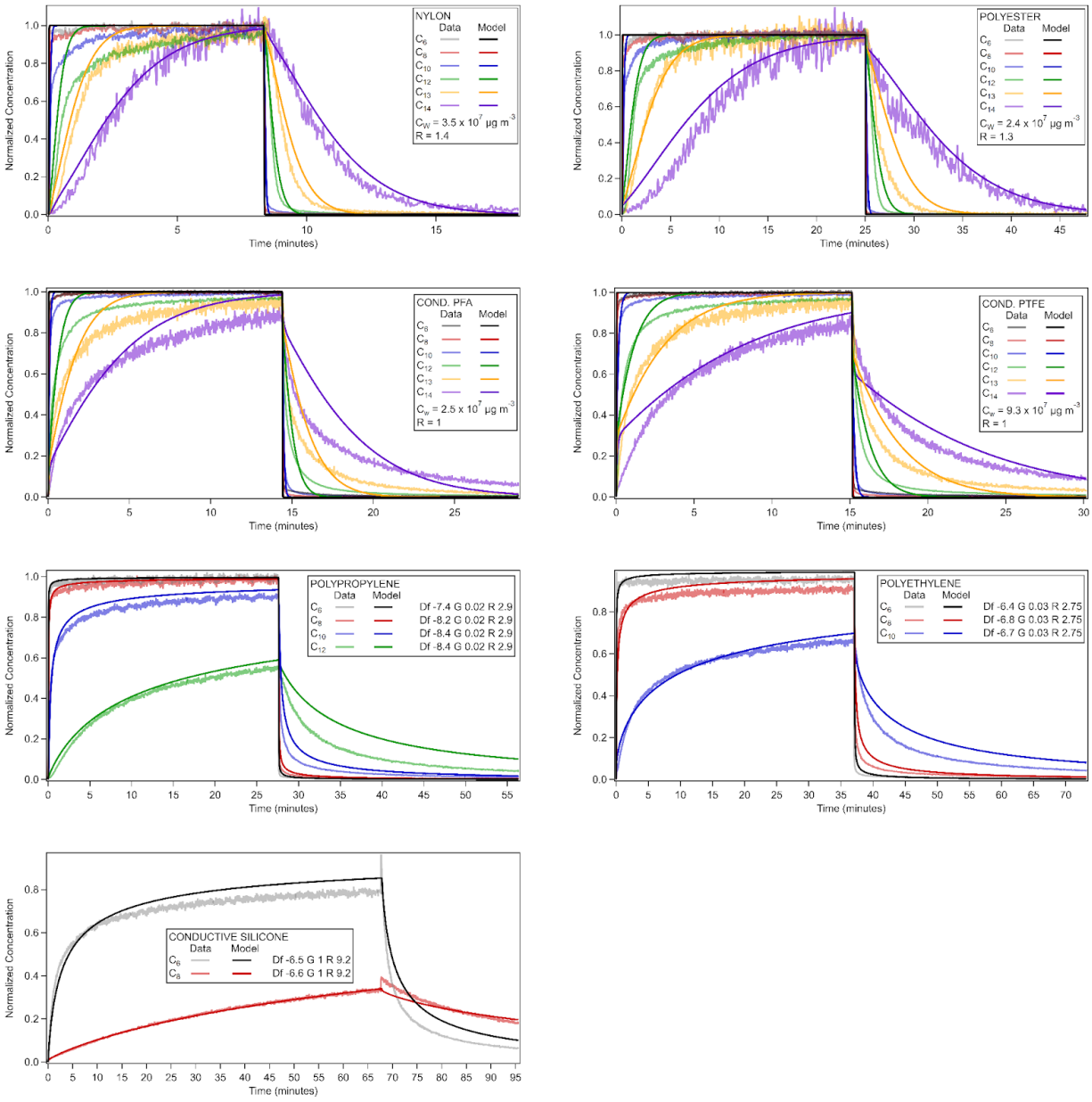

Figure S5. Final model fits for the materials in this study, with the optimized fitting parameters listed.

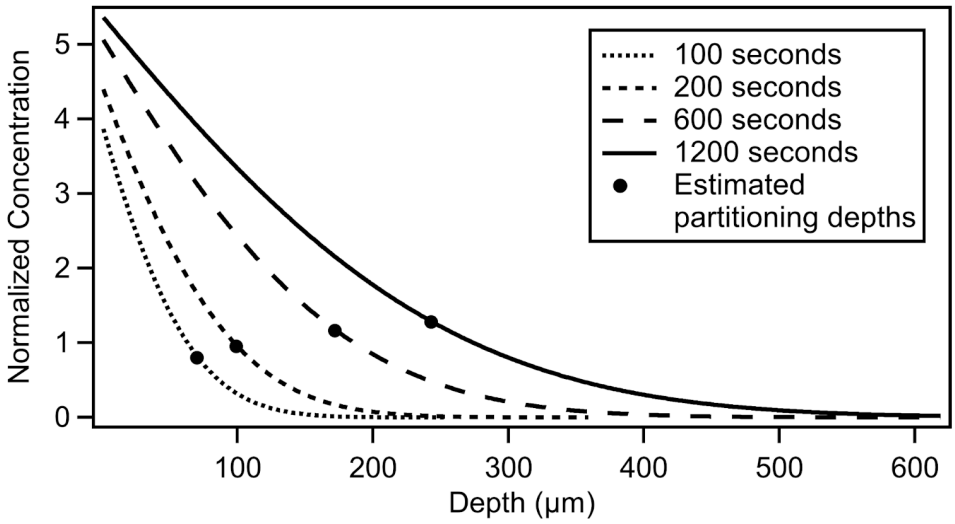

Figure S6. Results from multilayer model runs, showing concentration as a function of depth into the tubing wall, over time. The model is simulating C_{10} ketone absorbing into polyethylene tubing. To calculate a partitioning depth, both the absorption timescale and concentration threshold need to be considered. We use Eq. 6 from Algrim et al. (2020) to estimate the partitioning depths reported in Table 2, which are shown in this plot as markers.

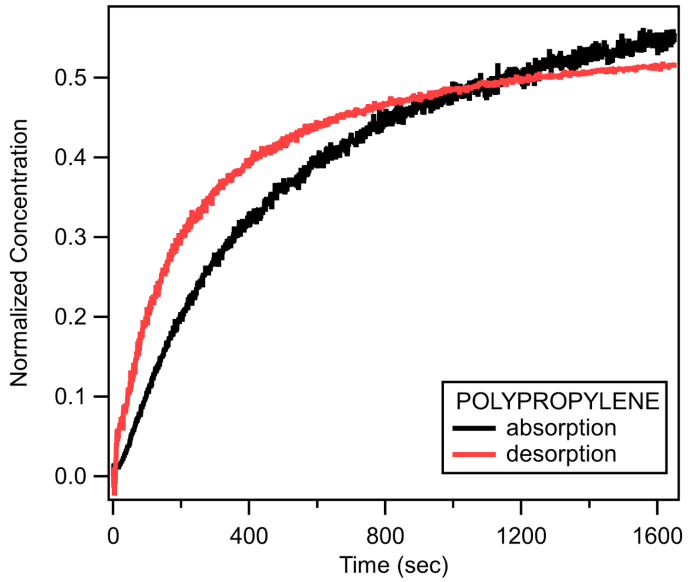

Figure S7. Measured absorption and desorption profiles for the C_{12} ketone in polypropylene tubing, with the desorption profile flipped to compare with the absorption profile. Crossing profiles of this nature are considered anomalous in the polymer diffusion literature, and the multilayer model was not designed to simulate this behavior (see main text).

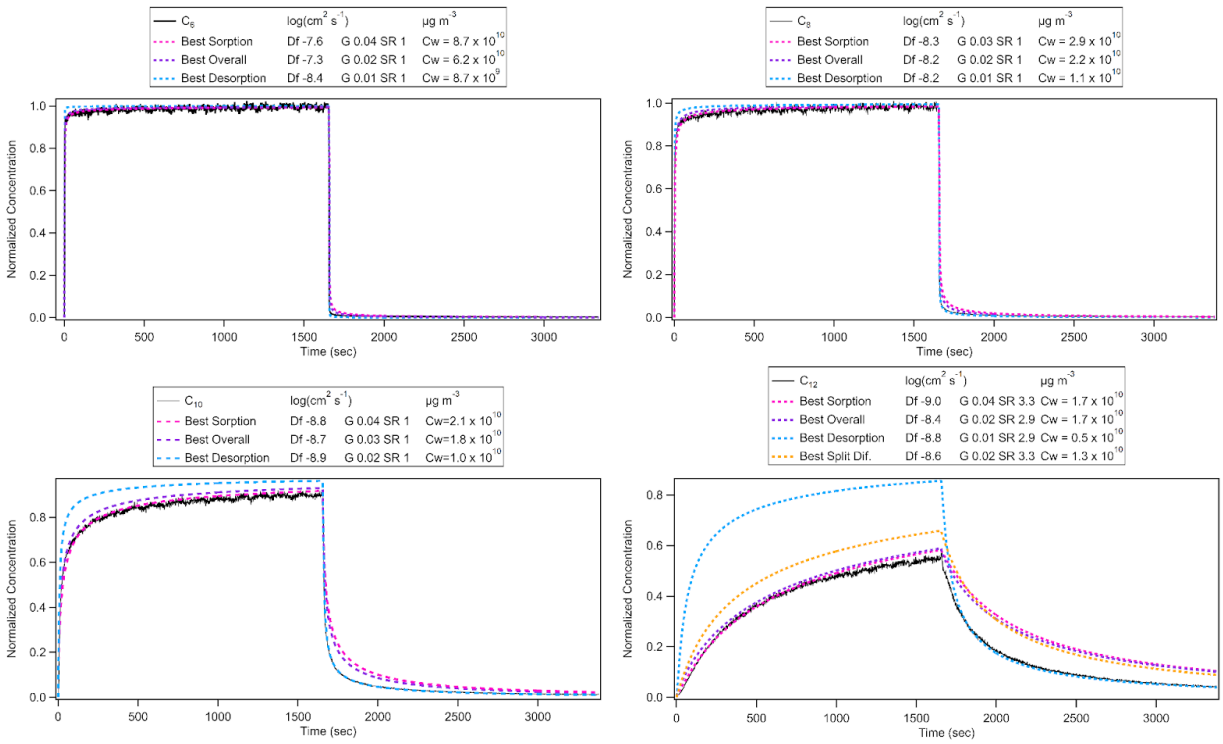

Figure S8. Experimental and modeled time series of C_6, C_8, C_{10} and C_{12} ketones through polypropylene tubing, for comparison. Pink traces are the best fits for absorption period and blue traces are the best fit for desorption period. Purple traces minimize the overall error (and were the ones chosen for final fitting parameters). Here we demonstrate that it is possible to fit both the absorption and desorption periods individually using the model, but finding a model run that minimizes total error requires splitting the difference in error between the two periods. For the C_{12} ketone, there is an additional yellow trace, where the absorption fit error and desorption fit error are equal. Due to the asymmetry in the experimental data, we can significantly reduce the error during the absorption period, while slightly increasing the error for the desorption period, to reduce the total error significantly. This is why the best fit trace (purple) is not the same as the yellow trace.

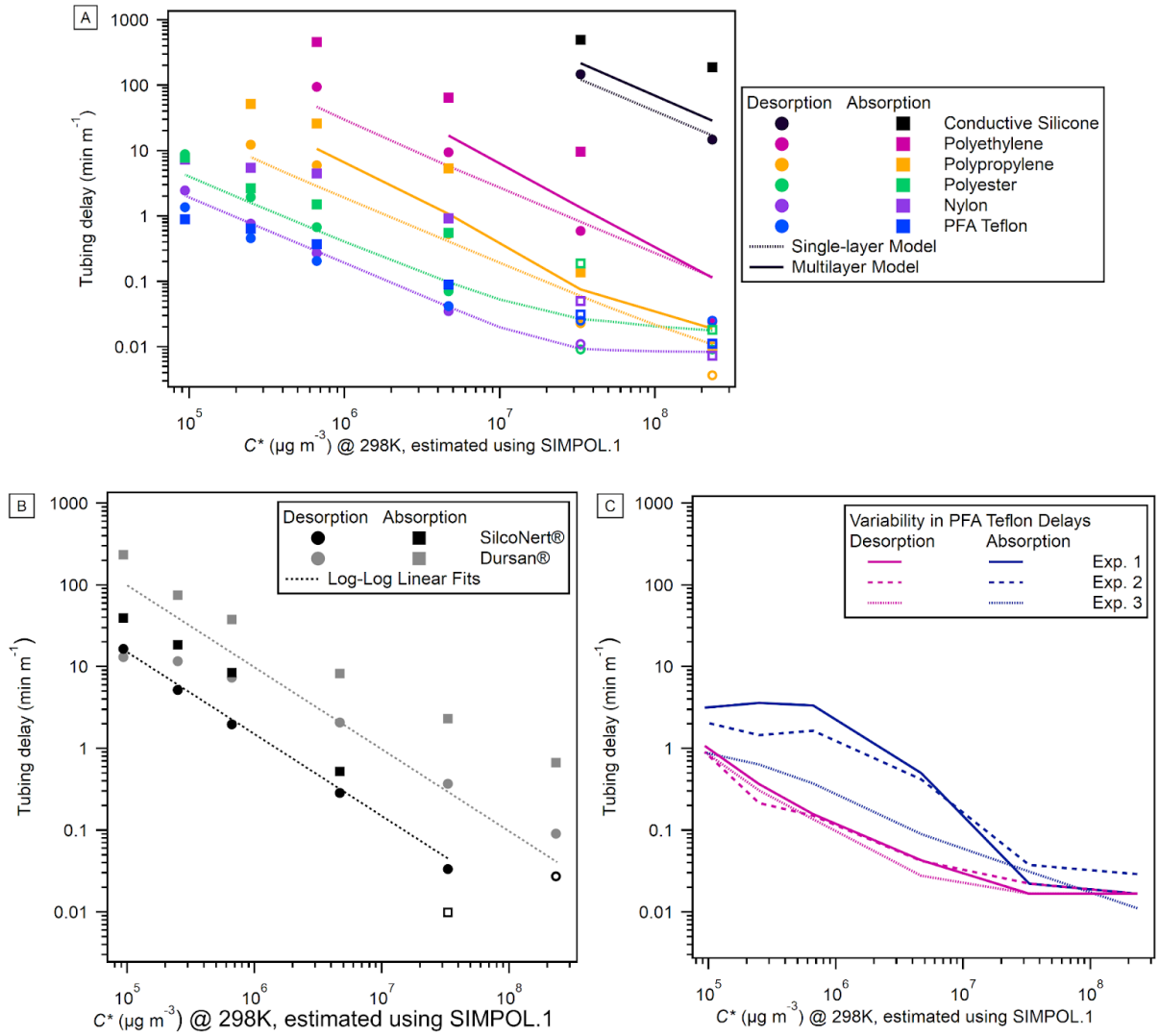

Figure S9. A) A comparison of delay times calculated using either the desorption period or the absorption period for the polymer materials in this study. Open markers indicate delays that may be smaller than the 1 second measurement limitation. Absorption delay times are slightly higher across all materials than desorption delay times. B) A comparison of delays times calculated using either the desorption period or the absorption period for the metal tubes in this study. C) Delays in PFA calculated from three different experiment days using the desorption and absorption periods. There was less run to run variability in the desorption-calculated times than the absorption-calculated times.

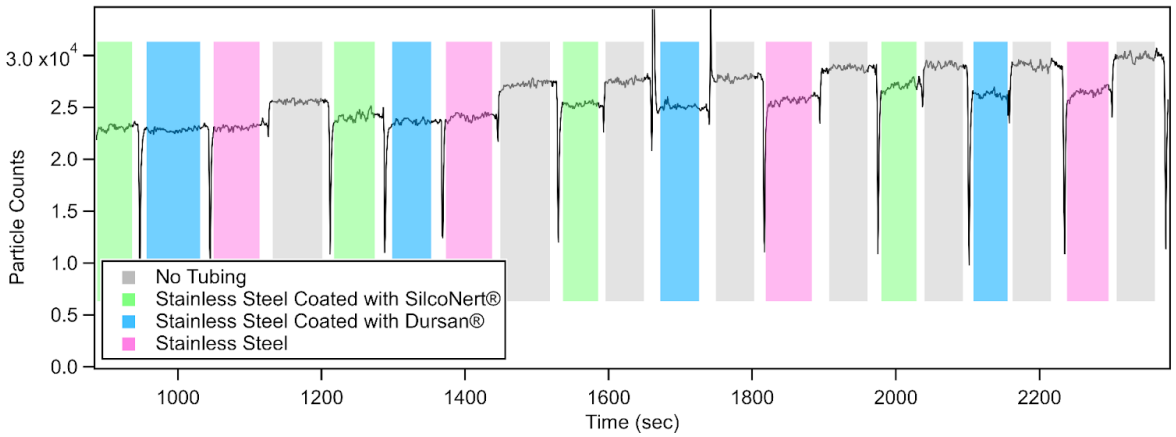

Figure S10. Time series showing the transmission of room particles to a condensation particle counter through the steel tubes (coated and uncoated). Spikes during transition periods are due to temporary pressure changes while switching valves.

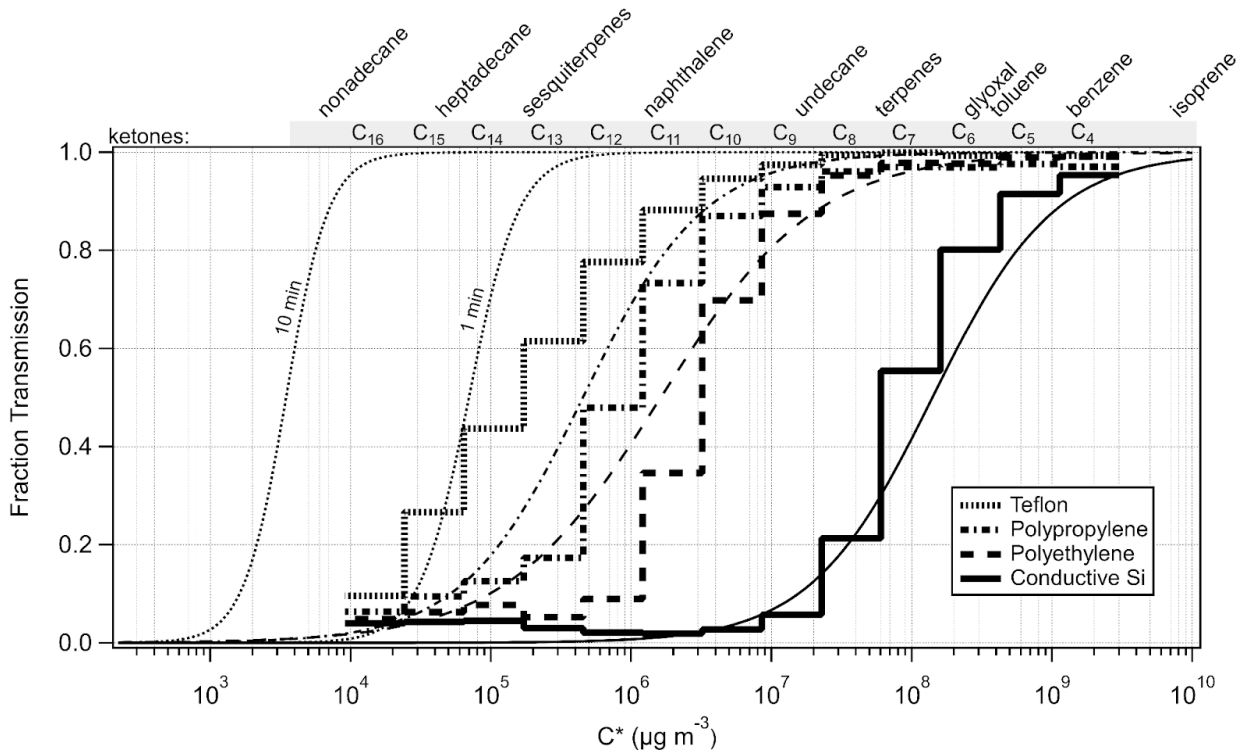

Figure S11. Cityscape lines are experimental fraction transmission through the GVS after about 10 minutes of sampling, according to *C**, for various polymer tubing materials. Smooth lines show model runs for 10 minutes, unless otherwise labeled. PFA was modeled with the single layer model, and the other materials were modeled with the multilayer model. Since the multilayer model requires an input solid-phase diffusion coefficient for every input saturation vapor pressure, a linear relationship was derived from Algrim et al. (2020), shown in Fig. 4. See main text for discussion of the PFA modeling.

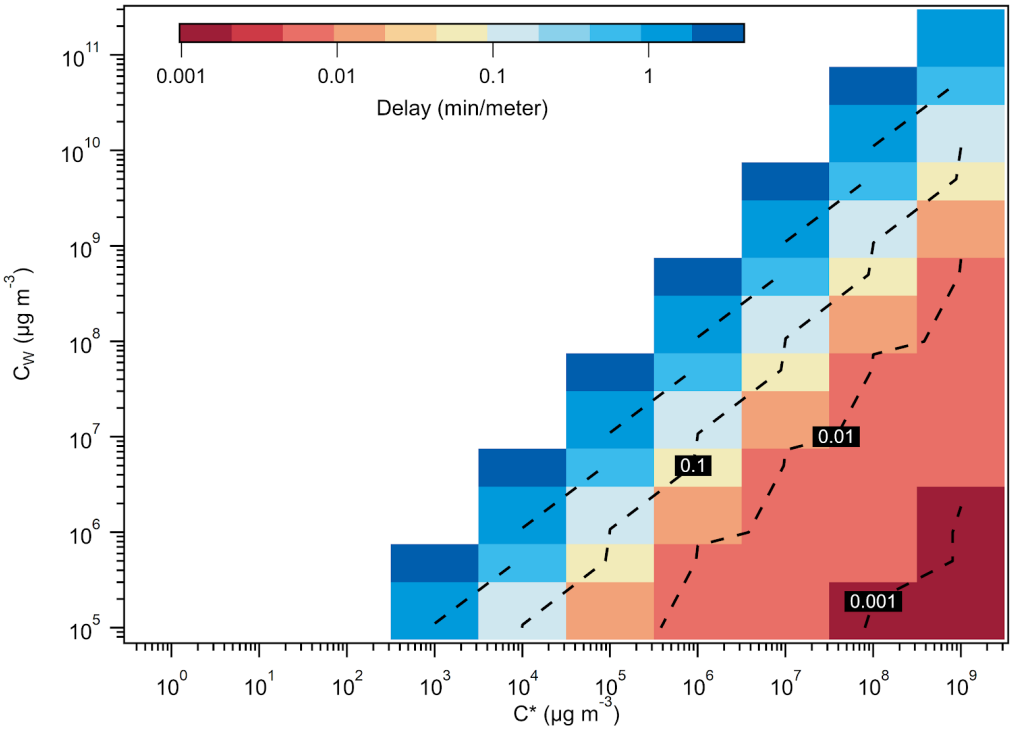

Figure S12. Guide for using simple tubing materials to achieve a volatility separation prior to detection. The vertical axis is the absorptive capacity (of a material), and the horizontal axis is saturation mass concentration (of a compound). The data is colored according to the delay time for a given compound volatility sampled through a material with a given absorptive capacity. The single layer model was run using a flow rate of 2 L min^{-1} and all tubing was modeled with an inner diameter of 0.3175 cm. Values for delays are expected to increase parallel to the model runs shown, but were not run due to computation time.

Experimental Comparison of Coated and Uncoated Oxidation Flow Reactors

Gas and particle transmission tests were completed for an uncoated (aluminum with chromate finish) and coated (same with commercial conductive PTFE-based coating) Aerodyne oxidation flow reactors (OFRs). The goal was to compare their performance in transmitting gases and particles. Results for tubing have shown that conductive Teflon has much better gas transmission than the aluminum-chromate material, while particle transmission is similar. Therefore we decided to explore if this result is transferable to the OFR conductive Teflon coating (which is different from the tubing material).

There are several aspects that can be configured in the OFRs (see Fig. S13 for photos); in these tests, two (non-conductive, transparent) Teflon lamp sleeves were installed in each OFR, the inlet screens were removed, the input flow rate was 4.4 LPM, and the output flow rates were nominally 2 LPM through the center port, and 2.4 LPM through the outer ring port. All transmission tests monitored the center port. For the particle transmission measurements, inlets and outlets used stainless steel fittings, as shown in Fig. S13B, to reduce particle losses in those connections. For the gas transmission work, the inlets and outlets were changed to PFA Teflon, as shown in Fig. S13C, to reduce compound partitioning to the wall material in those connections. Some of the gas phase tests were completed with a small 2.5 cm x 2.5 cm fan (Coolerguys, Part No. 840556070306) installed inside the OFR (shown in Fig. S13D). While this is not how OFRs are configured in laboratory or field work, it provided us the opportunity to greatly enhance mixing and thus surface contact in the OFR, to more clearly ascertain possible coating effects on gas transmission. Without the fan, gas transmission was convolved with the air flow residence time distribution in the OFR, and with the fan, compounds were immediately well-mixed, likely with increased wall interactions, and then exponentially decayed as they were cleared. Therefore, results shown with the fan installed are a "worst-case scenario" for transmission, as they maximize gas-wall interactions.

To test for particle transmission, the OFRs were plumbed to a large environmental chamber containing ~115 μg m^{-3} of dioctyl sebacate (DOS). A scanning mobility particle sizer (SMPS) was used to monitor the particle input and output of the OFR, from which transmission according to particle size can be derived. The time series in Fig. S14 shows that particle transmission, on a volume basis, was 90.2% through the uncoated OFR, and 83.9% through the coated OFR, for the particle size distributions sampled. Figure S15 shows the distributions of particles that were sampled over time. Most particle volume was in the range of ~100-350 nm.

To test for gas transmission, the OFRs drew air from a chamber containing 20-40 ppb each of isoprene and C_6-C_{14} 2-ketones (with a saturation concentration range of C^* ~ 10^4 - 10^8 μg m^{-3}), and a Vocus proton-transfer-reaction mass spectrometer was used to monitor transmission. Isoprene was added as a non surface-interactive tracer to track the residence time distribution of each experiment (due to its high volatility). Two types of experiments were conducted, the first being a burst-style experiment, where the OFRs sampled compounds from the chamber for about 10 seconds, and otherwise sampled clean air (with RH = ~25%). This experiment was performed for both OFRs, with and without the fan installed inside. Results from the burst-style experiment

are shown in Fig. S16; the coated OFR had a slightly faster time response to the ketones. The second style of experiment was a steady-state experiment, in which the OFRs sampled the compounds continuously for about 10 minutes, with the fan installed. Results from the steady-state experiments are shown in Fig. S17; the coated OFR showed slightly more sorption compared to the uncoated OFR.

Both the uncoated and the coated OFRs transmitted particles and gases with relatively high efficiency. Gas transmission through both was dependent on compound volatility, with higher volatility compounds transmitting faster, as expected. The uncoated OFR performed better than the coated OFR in the steady-state, fan-in, experiment, while the coated OFR performed better in the burst-style experiments. We hypothesize that this is due to the difference in sorptive processes occuring in each. In the uncoated OFR, adsorption is likely occurring (compounds can only occupy surface sites), which may cause extended partitioning in a burst experiment, but would saturate with compounds in a steady-state experiment more quickly than an absorptive material. Alternatively, in the coated OFR, absorption is likely occurring (compounds can diffuse into the coating material), which may respond quickly in a burst experiment, but would take longer to saturate in a steady-state experiment compared to an adsorptive material. Since the steady-state experiments were run with the fan, we expect that when the air flow and residence time distribution is established as normal (no fan), transmission would be faster, as gas-wall interactions would be reduced. The coated OFR is specifically preferred over the chromated aluminum OFR when halogen chemistry is of interest, as the coating is inert to halogens.

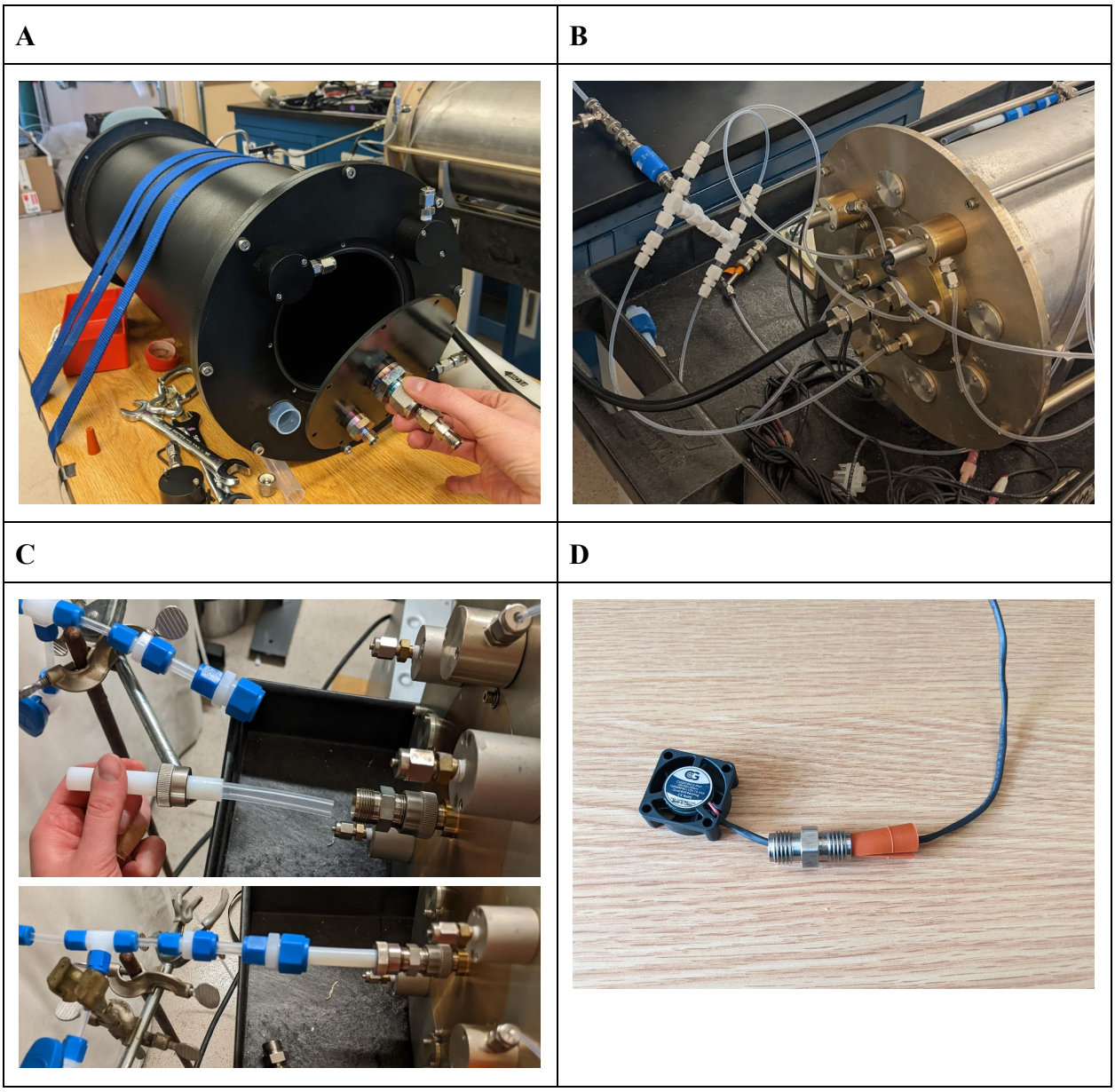

Figure S13. Photos describing OFR configuration for various tests. A) Front plate of coated OFR, which has a primary and secondary inlet port. One of two Teflon sleeves can be seen in the bottom left lamp port. B) Uncoated OFR with stainless steel outlet (identical inlet was used) to conductive silicone tubing for particle experiments. C) Teflon inlet (identical outlet was used) for gas experiments. Nested Teflon tubing of a smaller diameter was used to "bore through" the full inlet length to minimize exposed metal (to reduce partitioning interference). D) Demonstration of how the fan was installed and sealed. The fan went inside the OFR, and the wire was fed through the secondary inlet port on the front plate (shown in A), and was sealed in with a rubber ¼" plug from the outside. The ¼" union shown represents the secondary inlet port in the actual setup.

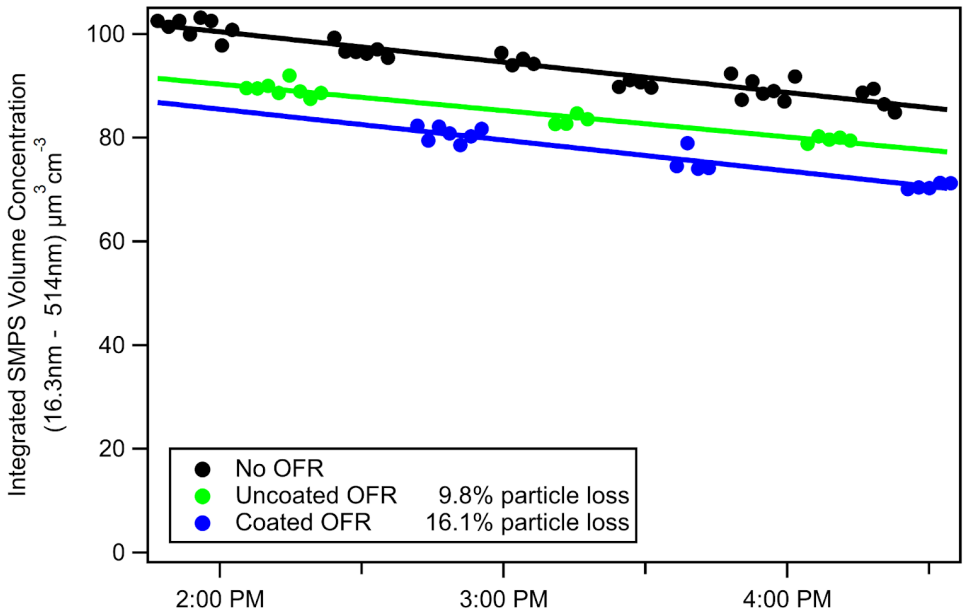

Figure S14. Steady-state particle transmission time series, where dioctyl sebacate particles were sampled from a chamber alternately through both OFRs and a sample line without an OFR. The OFRs were kept passivated by constantly flowing air through the ring ports, and switching open the center ports when it was time to measure. Percent particle loss by volume is reported.

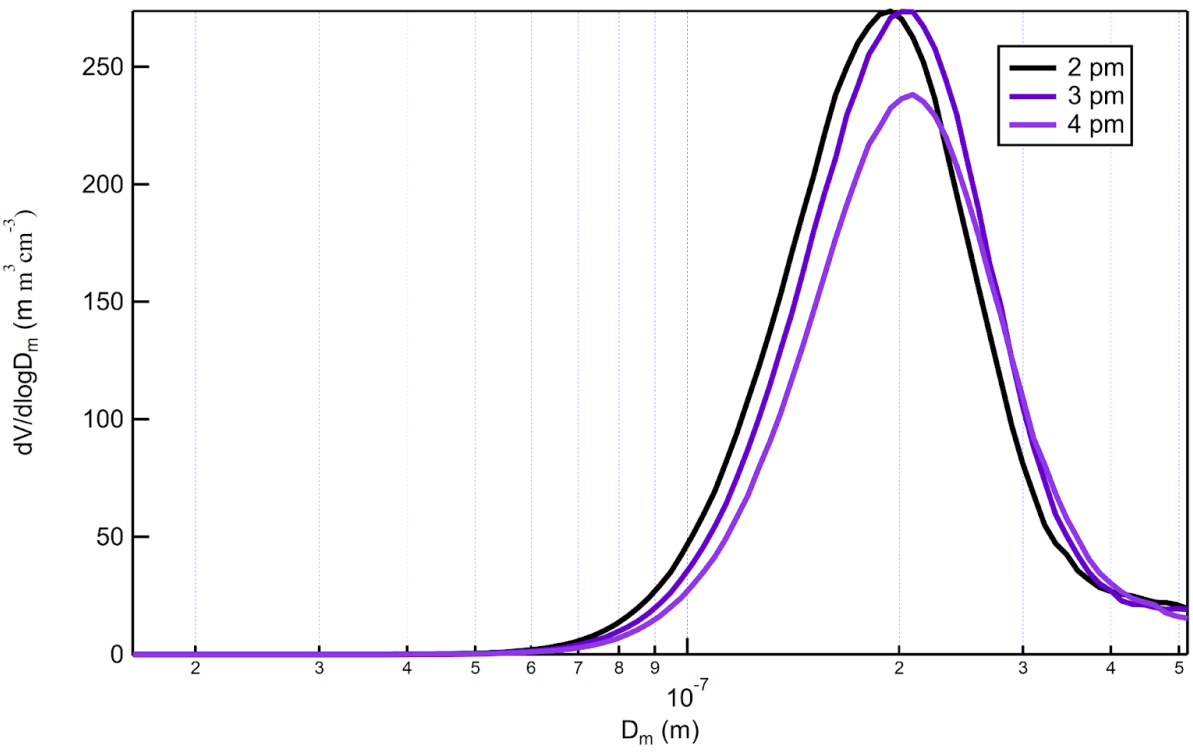

Figure S15. Particle volume distribution, as measured with an SMPS, over time during steady-state particle experiment from Fig. S14.

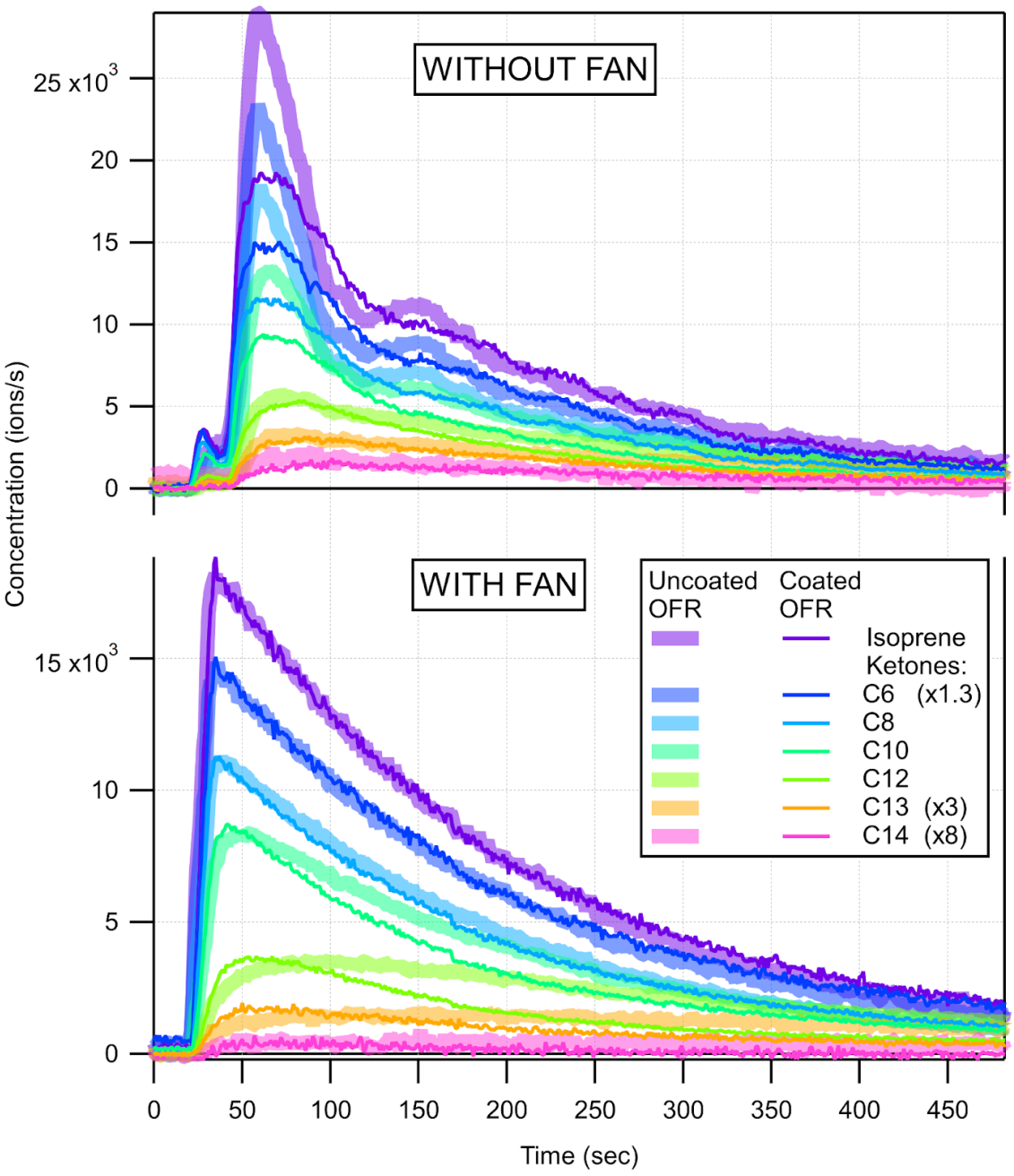

Figure S16. Time series of burst-style gas transmission experiments, where the OFRs sampled compounds for 10 seconds, and otherwise sampled clean air. Top shows gas transmission without fan installed, and bottom shows gas transmission with fan installed (which represents a "worst-case scenario" for gas-wall interactions). The coated OFR shows slightly better time response than the uncoated OFR.

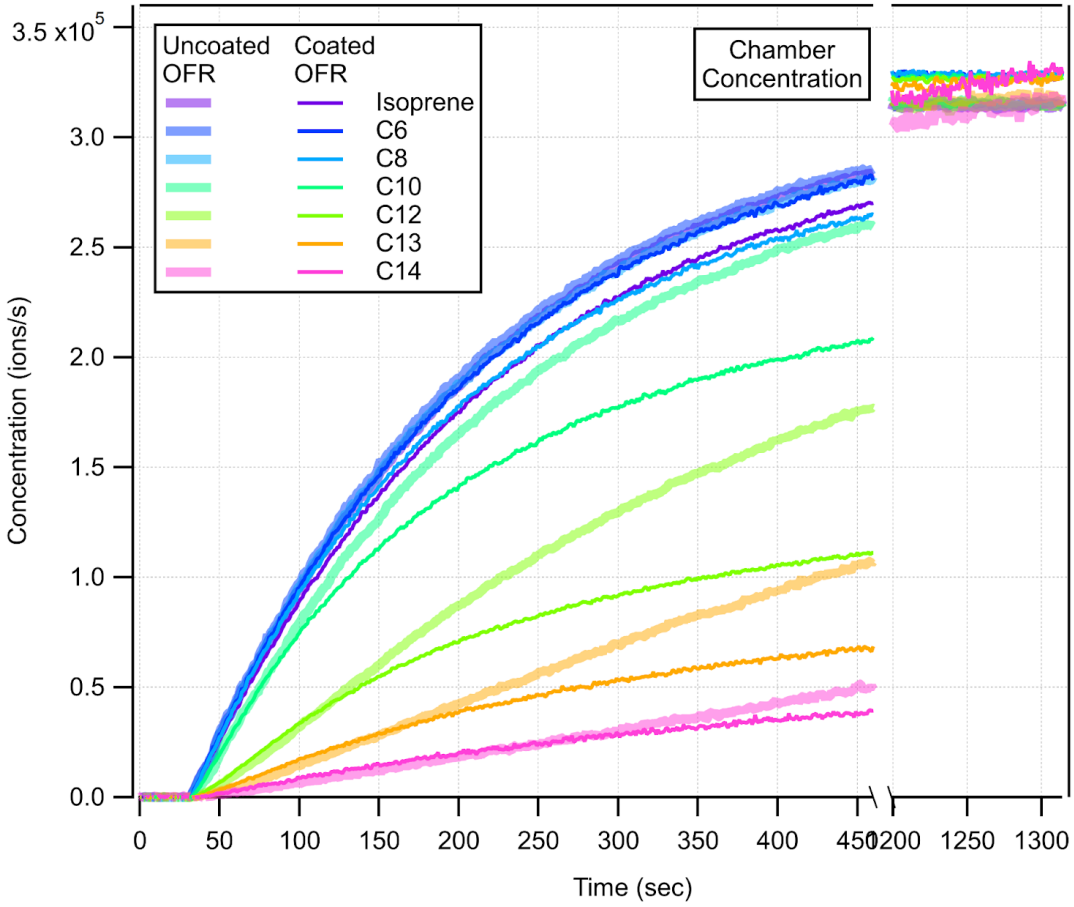

Figure S17. Time series of steady-state gas transmission experiments through both OFRs while running the fan (which represents a "worst-case scenario" for gas-wall interactions). Chamber concentrations are shown on the right. Uncoated OFR (which likely *adsorbs* compounds) shows slightly less sorption than coated OFR (which likely *absorbs* compounds). For both OFRs, the amount of sorption increases as compound volatility decreases.

References

Algrim, L. B., Pagonis, D., de Gouw, J. A., Jimenez, J. L., and Ziemann, P. J.: Measurements and modeling of absorptive partitioning of volatile organic compounds to painted surfaces, Indoor Air, 30, 745–756, https://doi.org/10.1111/ina.12654, 2020.

Huang, Y., Zhao, R., Charan, S. M., Kenseth, C. M., Zhang, X., and Seinfeld, J. H.: Unified Theory of Vapor-Wall Mass Transport in Teflon-Walled Environmental Chambers, Environ. Sci. Technol., 52, 2134–2142, https://doi.org/10.1021/acs.est.7b05575, 2018.

Manuja, A., Ritchie, J., Buch, K., Wu, Y., Eichler, C. M. A., Little, J. C., and Marr, L. C.: Total surface area in indoor environments, Environ. Sci. Process. Impacts, 21, 1384–1392, https://doi.org/10.1039/c9em00157c, 2019.